Acta Crystallographica Section D
Biological Crystallography
ISSN 0907-4449

Structural and functional characterization of HP0377, a thioredoxin-fold protein from *Helicobacter pylori*

Ji Young Yoon,[a] Jieun Kim,[b] Doo Ri An,[b] Sang Jae Lee,[c] Hyoun Sook Kim,[a,c] Ha Na Im,[b] Hye-Jin Yoon,[a] Jin Young Kim,[d] Soon-Jong Kim,[e] Byung Woo Han[c]* and Se Won Suh[a,b]*

[a]Department of Chemistry, College of Natural Sciences, Seoul National University, Seoul 151-742, Republic of Korea, [b]Department of Biophysics and Chemical Biology, College of Natural Sciences, Seoul National University, Seoul 151-742, Republic of Korea, [c]College of Pharmacy, Seoul National University, Seoul 151-742, Republic of Korea, [d]Division of Mass Spectrometry, Korea Basic Science Institute, Ochang-eup Yeongudangiro 162, Cheongwon-gun, Chungbuk 363-883, Republic of Korea, and [e]Department of Chemistry, Mokpo National University, Chonnam, Republic of Korea

Correspondence e-mail: bwhan@snu.ac.kr, sewonsuh@snu.ac.kr

Received 11 July 2012
Accepted 12 January 2013

PDB References: partially oxidized HP0377, 4fyb; reduced HP0377, 4fyc

Maturation of cytochrome *c* is carried out in the bacterial periplasm, where specialized thiol-disulfide oxidoreductases provide the correct reduction of oxidized apocytochrome *c* before covalent haem attachment. HP0377 from *Helicobacter pylori* is a thioredoxin-fold protein that has been implicated as a component of system II for cytochrome *c* assembly and shows limited sequence similarity to *Escherichia coli* DsbC, a disulfide-bond isomerase. To better understand the role of HP0377, its crystal structures have been determined in both reduced and partially oxidized states, which are highly similar to each other. Sedimentation-equilibrium experiments indicate that HP0377 is monomeric in solution. HP0377 adopts a thioredoxin fold but shows distinctive variations as in other thioredoxin-like bacterial periplasmic proteins. The active site of HP0377 closely resembles that of *E. coli* DsbC. A reductase assay suggests that HP0377 may play a role as a reductase in the biogenesis of holocytochrome c_{553} (HP1227). Binding experiments indicate that it can form a covalent complex with HP0518, a putative L,D-transpeptidase with a catalytic cysteine residue, *via* a disulfide bond. Furthermore, physicochemical properties of HP0377 and its R86A variant have been determined. These results suggest that HP0377 may perform multiple functions as a reductase in *H. pylori*.

1. Introduction

Archaea, bacteria, fungi, plant thylakoids and almost all higher organisms use *c*-type cytochromes for electron transfer in a multitude of different cellular processes (Barker & Ferguson, 1999; Page *et al.*, 1998; Thöny-Meyer, 1997; Pettigrew & Moore, 1987; Moore & Pettigrew, 1990; Scott & Mauk, 1995). In addition, cytochromes *c* are involved in apoptosis in higher organisms (Martinou *et al.*, 2000). In *c*-type cytochromes, the haem vinyl groups are covalently ligated to the cysteine residues of the C*XX*CH motif (Hamel *et al.*, 2009). This haem ligation requires specific assembly proteins in prokaryotes or eukaryotic mitochondria and chloroplasts (Beckett *et al.*, 2000). Biogenesis of cytochrome *c* occurs in the bacterial periplasm, mitochondrial intermembrane space and thylakoid lumen. It consists of the following steps: (i) synthesis and transport across at least one biological membrane of apocytochrome *c* and haem and (ii) reduction and maintenance of the haem ferrous iron and the C*XX*CH sulfhydryls prior to (iii) the formation of thioether bonds between the haem and apocytochrome *c* (Hamel *et al.*, 2009; Ferguson *et al.*, 2008; Giegé *et al.*, 2008; Kranz *et al.*, 2009).

For the synthesis of cytochrome *c*, three distinct pathways called systems I, II and III have been reported (Thöny-Meyer, 1997; Kranz *et al.*, 1998; Page *et al.*, 1998). Bacteria

predominantly use systems I and II, whereas eukaryotes exclusively adopt system III. Many Gram-negative bacteria (including *Escherichia coli*), archaea and plant mitochondria use the system I pathway encoded by *ccm* (cytochrome *c* maturation) genes. System I is the most studied pathway and involves thiol reduction of apocytochrome *c* by a specific periplasmic thioredoxin-like protein called CcmG (or HelX; Beckman & Kranz, 1993; Page & Ferguson, 1997; Monika *et al.*, 1997), which itself is reduced by the transmembrane DsbD (or the related CcdA; Missiakas *et al.*, 1995; Metheringham *et al.*, 1996; Turkarslan *et al.*, 2008). Other proteins are involved in haem export (CcmABCD), haem chaperoning (CcmE), apocytochrome trafficking and thiol reduction (CcmH) and haem reduction (CcmF) prior to attachment of haem to apocytochrome *c* by the CcmF/H complex (Kranz *et al.*, 2009; Sanders *et al.*, 2010). System II, referred to as the 'CCS' (cytochrome *c* synthesis) pathway, is present in some Gram-negative bacteria (*e.g. Helicobacter* and *Wolinella*), Gram-positive bacteria (e.g. *Mycobacterium* and *Bacillus*), cyanobacteria and chloroplasts. System II is comprised of four (sometimes three) membrane-bound proteins: CcsA (ResC) and CcsB (ResB) are the components of the cytochrome *c* synthase, whereas CcdA and CcsX (ResA) function in the generation of a reduced haem *c* attachment motif (Simon & Hederstedt, 2011). The CcdA protein that corresponds to the transmembrane domain of DsbD is required for reducing CcsX (ResA) and receives its reducing equivalents from thioredoxin in the cytoplasm (Deshmukh *et al.*, 2000; Möller & Hederstedt, 2008). In a few bacteria such as *Helicobacter*, *Bacteroides* and *Wolinella*, the genes encoding the CcsB and CcsA proteins are naturally fused into one large ORF (called *ccsBA*). The integral membrane protein CcsBA acts as a haem exporter and attaches haem to apocytochrome *c* (Frawley & Kranz, 2009). System III is the simplest pathway, consisting of cytochrome *c* haem lyase (CCHL; Dumont *et al.*, 1987; Nicholson *et al.*, 1987; Zollner *et al.*, 1992). CCHL synthesizes holocytochrome *c* and has been also called holocytochrome *c* synthase (HCCS), cytochrome *c* synthase or cytochrome *c* synthetase (Schaefer *et al.*, 1996; Prakash *et al.*, 2002; Schwarz & Cox, 2002).

In *H. pylori* 26695, homologous genes for a system I cytochrome *c* biogenesis pathway were not found, but homologues of the four proteins of system II were identified (Goldman & Kranz, 1998). HP0265 is homologous to the CcdA protein of *B. subtilis* (Goldman & Kranz, 1998). HP0378 contains homologues of two system II components (CcsB and CcsA proteins) in a single open reading frame. It contains a homologue of cyanobacterial Ccs1 (also called CcsB or ResB) at the N-terminus and a homologue of the CcsA (ResC) protein from *Chlamydomonas reinhardtii* (Goldman & Kranz, 1998). HP0377, a thioredoxin-like protein located directly upstream of HP0378 in a single operon (Sharma *et al.*, 2010), is homologous to the ResA protein of *B. subtilis* (15% overall sequence identity), which is required to keep the cysteine residues in the haem-binding C*XX*CH motif of apocytochrome *c* reduced before haem attachment. Since HP0378 is homologous to CcsBA and plays a role in the system II pathway (Feissner *et al.*, 2006), HP0377 may play a similar role to *B. subtilis* ResA. HP0377 is presently annotated as a putative *H. pylori* DsbC in the ExPASy database because it was identified as a homologue of the *E. coli* disulfide-bond isomerase DsbC (12% overall sequence identity; Kaakoush *et al.*, 2007). However, no detailed functional and structural characterizations of HP0377 have been reported.

To elucidate the role of HP0377 as a component of the *H. pylori* system II in cytochrome *c* biogenesis, we have determined its crystal structures in both reduced and partially oxidized states. HP0377 possesses a classic thioredoxin fold with a distinct insertion between $\alpha2$ and $\beta2$ and extensions at both the N- and C-termini. It exists as a monomer in solution as indicated by sedimentation-equilibrium analysis. It also exists as monomers in the crystal. Other periplasmic thioredoxin-like proteins (*e.g. B. subtilis* ResA, *Bradyrhizobium japonicum* CcmG and TlpA, and *E. coli* CcmG) also exist as monomers (Crow *et al.*, 2004; Edeling *et al.*, 2002, 2004; Capitani *et al.*, 2001). In contrast, the DsbCs from *E. coli* and *Haemophilus influenzae* are V-shaped dimeric proteins. Despite the difference in oligomeric state, the active sites of HP0377 and *E. coli* DsbC are remarkably similar to each other. Furthermore, we show that HP0377 may function as a reductase to reduce oxidized apocytochrome c_{553} (HP1227). No substantial difference is observed between the reduced and partially oxidized structures of HP0377. This is in contrast to *B. subtilis* ResA, which undergoes a noticeable conformational change according to the redox state to recognize its specific substrate, apocytochrome *c* (Crow *et al.*, 2004). We also show that HP0377 can form a covalent complex with a putative L,D-transpeptidase (HP0518) from *H. pylori*, which contains a single cysteine residue in the active site. Moreover, physicochemical properties of HP0377 as well as of its R86A variant, such as the insulin-reducing activity, the redox potential, the thermodynamic stability and the pK_a of the active-site cysteine residue, have been measured in order to understand the function of HP0377 and the role of Arg86. Our structural and functional characterizations of HP0377 provide insights into its potential role in the system II cytochrome *c* biogenesis pathway and its DsbC-like function in *H. pylori*. These results, together with the relatively small size of the *H. pylori* genome, suggest that HP0377 may have evolved to carry out multiple functions in *H. pylori*.

2. Materials and methods

2.1. Cloning, expression and purification of HP0377

The gene encoding the N-terminally truncated form of *H. pylori* HP0377 was PCR-amplified and cloned into the expression vector pET-28b(+) (Novagen) using the restriction enzymes *Nde*I and *Xho*I. We tested three constructs covering residues 24–221, 28–221 and 33–221. The 24–221 construct contained an eight-residue hexahistidine-containing tag (LEHHHHHH) at the C-terminus, while the 28–221 and 33–221 constructs contained a 21-residue hexahistidine-containing tag (MGSSHHHHHHSSGLVPRGSHM) at the N-terminus. The

Table 1
Statistics of data collection, phasing and model refinement.

Values in parentheses are for the highest resolution shell.

	SeMet	Reduced	Oxidized
Data collection			
Data set	SAD [Se peak]	Native	Native
Space group	*C*2	*C*2	*C*2
Unit-cell parameters (Å, °)	a = 134.4, b = 44.0, c = 80.1, $\alpha = \gamma = 90$, β = 108.9	a = 140.9, b = 44.0, c = 76.7, $\alpha = \gamma = 90$, β = 112.3	a = 133.6, b = 43.9, c = 80.1, $\alpha = \gamma = 90$, β = 108.7
X-ray wavelength (Å)	0.97895	1.0000	1.2398
Resolution range (Å)	20–2.40 (2.49–2.40)	20–2.30 (2.34–2.30)	20–2.20 (2.28–2.20)
Total/unique reflections	249323/33479†	73460/17837	98913/22514
Completeness (%)	99.6 (100.0)†	93.2 (83.3)	99.4 (95.4)
$\langle I\rangle/\langle\sigma(I)\rangle$	49.1 (9.7)†	38.1 (4.8)	23.0 (2.4)
$R_{\rm merge}$‡ (%)	7.7 (34.2)†	4.3 (27.9)	7.6 (40.6)
SAD phasing			
Figure of merit (before/after density modification)			0.33/0.62
Model refinement			
Resolution range (Å)		20.0–2.30	20.0–2.20
$R_{\rm work}/R_{\rm free}$§ (%)		19.1/23.8	19.5/23.0
Monomers per asymmetric unit		2	2
Unique reflections used in the $R_{\rm free}$ set§		910	1154
No. of non-H atoms/average B factor (Å^2)			
Protein		2633/50.8	2647/42.3
Water		63/46.0	131/41.4
Glycerol		—	6/72.5
PEG		13/69.3	—
Wilson B factor (Å^2)		44.6	36.6
R.m.s. deviations from ideal geometry			
Bond lengths (Å)		0.009	0.008
Bond angles (°)		1.20	1.15
R.m.s. Z scores¶			
Bond lengths		0.421	0.401
Bond angles (°)		0.541	0.516
Ramachandran plot (including Gly and Pro)††			
Favoured (%)		98.4	98.4
Allowed (%)		1.6	1.6
Rotamer outliers†† (%)		0.7	0.7

† Values obtained by treating Friedel pairs as separate observations. ‡ $R_{\rm merge} = \sum_{hkl}\sum_i |I_i(hkl) - \langle I(hkl)\rangle|/\sum_{hkl}\sum_i I_i(hkl)$, where $I(hkl)$ is the intensity of reflection hkl, $\sum_{hkl}$ is the sum over all reflections and $\sum_i$ is the sum over i measurements of reflection hkl. § $R = \sum_{hkl}\big||F_{\rm obs}| - |F_{\rm calc}|\big|/\sum_{hkl}|F_{\rm obs}|$, where $R_{\rm free}$ and $R_{\rm work}$ are calculated for a randomly chosen 5% of reflections that were not used for refinement and for the remaining reflections, respectively. ¶ Values obtained using *REFMAC*. †† Values obtained using *MolProbity*.

24–221 construct was expressed and purified to confirm its oligomeric state in solution by sedimentation equilibrium. The expressed 28–221 construct was largely insoluble and could not be purified. The expressed 33–221 construct was purified and was used for crystallization and biochemical characterizations.

The recombinant protein was overexpressed in *E. coli* Rosetta2(DE3)pLysS cells using Terrific Broth culture medium. Protein expression was induced using 0.5 m*M* isopropyl β-D-1-thiogalactopyranoside (IPTG) and the cells were incubated for an additional 18 h at 303 K following growth to mid-log phase at 310 K. The cells were lysed by sonication in lysis buffer [20 m*M* Tris–HCl pH 7.9, 500 m*M* NaCl, 5%(*v*/*v*) glycerol] containing 5 m*M* imidazole followed by centrifugation to remove cellular debris. The supernatant was applied onto a HiTrap Chelating HP (GE Healthcare) affinity-chromatography column. The protein was eluted with lysis buffer containing 300 m*M* imidazole and the eluted sample was further purified by size-exclusion chromatography on a HiLoad 16/60 Superdex 200 prep-grade column (GE Healthcare). The elution buffer consisted of 20 m*M* Tris–HCl pH 7.2, 200 m*M* NaCl, 0.1 m*M* tris(2-carboxyethyl)phosphine (TCEP) hydrochloride (BioShop, Canada). Selenomethionine-labelled protein was expressed and purified as above, except that the M9 cell-culture medium which contained extra amino acids including selenomethionine (SeMet) was used. The crystal structures of the purified HP0377 (both the native and the SeMet derivative) were later found to be in the oxidized state. The reduced HP0377 protein sample for crystallization experiments was prepared by increasing the TCEP concentration in the elution buffer for size-exclusion chromatography to 1 m*M*. The crystal structure of this sample was later confirmed to be in the reduced state.

2.2. Crystallization and X-ray data collection of HP0377

For crystallization, the eluted HP0377 protein (residues 33–221) was concentrated to 20 mg ml^{-1} (832 μM) using an Amicon Ultra-15 centrifugal filter unit (Millipore). Crystals were grown by the sitting-drop vapour-diffusion method at 296 K. Each sitting drop was prepared by mixing 1 µl each of the protein solution and the reservoir solution and was placed over 100 µl reservoir solution. The best crystals of both SeMet-labelled and native HP0377 in the oxidized state were obtained with a reservoir solution consisting of 200 m*M* potassium acetate pH 7.8, 20%(*w*/*v*) polyethylene glycol (PEG) 1500, 2.2 m*M* FOS-Choline-8 (fluorinated). Crystals of reduced HP0377 were obtained in 200 m*M* sodium formate pH 7.0, 20%(*w*/*v*) PEG 3350. Crystals were transferred to a cryoprotectant solution consisting of 20%(*v*/*v*) glycerol in the reservoir solution. Single-wavelength anomalous diffraction (SAD) data were collected from a crystal of SeMet-substituted HP0377 at 100 K on an ADSC Quantum 270 CCD detector system (Area Detector Systems Corporation, Poway, California, USA) at the BL-1A experimental station of Photon Factory, Japan. Raw data were processed using the *HKL*-2000 program suite (Otwinowski & Minor, 1997). The crystal of SeMet-substituted HP0377 belonged to space group *C*2, with unit-cell parameters a = 134.4, b = 44.00, c = 80.07 Å, $\alpha = \gamma = 90$, β = 108.9°. Native X-ray data for the oxidized and reduced forms were collected at 100 K using an ADSC Quantum 210 CCD detector system on BL-6C of Pohang Light Source, Republic of Korea and using

an ADSC Quantum 270 CCD detector system at the BL-1A experimental station of Photon Factory, Japan, respectively. The native crystal of the oxidized form belonged to space group $C2$, with unit-cell parameters a = 133.6, b = 43.91, c = 80.06 Å, $\alpha = \gamma = 90$, $\beta = 108.7^\circ$, and the reduced form belonged to space group $C2$, with unit-cell parameters a = 140.9, b = 43.95, c = 76.70 Å, $\alpha = \gamma = 90$, $\beta = 112.3^\circ$. Both the oxidized and reduced forms contained two monomers per asymmetric unit, giving Matthews parameters and solvent contents of 2.31 Å^3 Da^{-1} and 46.9% for the oxidized form and of 2.30 Å^3 Da^{-1} and 46.2% for the reduced form, respectively (Table 1).

2.3. Structure determination and refinement

Phase calculation, density modification and initial model building were carried out using *AutoSol* and *AutoBuild* from the *PHENIX* suite of programs (Adams *et al.*, 2010). *AutoSol* located all six expected Se atoms of two HP0377 monomers in an asymmetric unit, except for that at the N-terminus. Subsequent manual model building was conducted using *Coot* (Emsley & Cowtan, 2004) and the model was refined with *REFMAC* (Murshudov *et al.*, 2011) and *PHENIX* (Adams *et al.*, 2010), including bulk-solvent correction. 5% of the data were randomly set aside as test data for calculation of $R_{\rm free}$ (Brünger, 1992). Water molecules were added using *Coot* and were manually inspected. The quality of the refined model was assessed by *MolProbity* (Chen *et al.*, 2010). Crystallographic and refinement statistics are summarized in Table 1. The coordinates and structure factors have been deposited in the Protein Data Bank under accession codes 4fyc for reduced HP0377 and 4fyb for partially oxidized HP0377.

2.4. Sedimentation equilibrium

Sedimentation-equilibrium experiments were performed using a Beckman ProteomeLab XL-A analytical ultracentrifuge in 20 m*M* Tris–HCl pH 7.2 buffer containing 200 m*M* NaCl and 1.5 m*M* TCEP at 293 K. Protein samples of HP0377 (33–221) at three different concentrations (7.9, 10.4 and 12.9 µ*M*) were analyzed at 20 000 rev min^{-1} by measuring the absorbance at 235 and 280 nm. The samples of HP0377 (24–221) were measured at two different speeds (20 000 and 24 000 rev min^{-1}) and at concentrations of 7.7 and 10.3 µ*M*. A six-sector cell was used with a loading volume of 140 µl. The protein concentration was calculated using ε_{280} = 19 370 M^{-1} cm^{-1} and a molecular mass of 24 027 Da for a monomer of HP0377 (33–221) fused with a 21-residue tag at the N-terminus. The concentration of HP0377 (24–221) was calculated using ε_{280} = 19 495 M^{-1} cm^{-1} and a molecular mass of 23 918 Da for the C-terminally histidine-tagged protein. The time required to attain equilibrium was established by running at the given rotor speed until the scans were invariant for 4 h; this was achieved after at most 60 h in the six-sector cell. The partial specific volume of the protein and the buffer density were calculated using *SEDNTERP* (Laue *et al.*, 1992). The calculated partial specific volumes of the protein at 293 K were 0.7271 and 0.7280 cm^3 g^{-1} for the 33–221 and 24–221 constructs, respectively; the buffer density was 1.00704 g cm^{-3}. For data analysis by mathematical modelling using nonlinear least-squares curve fitting, the following fitting functions were used for homogeneous models,

$$C_{\rm r} = C_{\rm b}\exp[A_{\rm p}M_{\rm p}(r^2 - r_{\rm b}^2)] + \varepsilon,$$
$$A_{\rm p} = (1 - \nu\rho)\omega^2/2RT, \quad (1)$$

where $C_{\rm r}$ is the total concentration at the radial position r, $C_{\rm b}$ is the concentration of protein at the cell bottom, $M_{\rm p}$ is the molecular mass of the protein, ν and ρ are the partial specific volume and the solution density, respectively, ω is the rotor angular velocity and ε is a baseline-error term. The selection of the model was made by examining the weighted sum or square values and the weighted root-mean-square error values. Further data manipulation and data analysis by mathematical modelling were performed using *MLAB* (Knott, 1979).

2.5. Preparation of apocytochrome c_{553} and *in vitro* reductase assay

The DNA sequence encoding the mature *H. pylori* cytochrome c_{553} (HP1227), excluding the signal peptide (Met1–Ala19), was PCR-amplified and cloned into the expression vector pET-21a(+) (Novagen) using the restriction enzymes *Nde*I and *Xho*I. The construct adds an eight-residue hexahistidine-containing tag (LEHHHHHH) at the C-terminus. The purification steps for *H. pylori* apocytochrome c_{553} were the same as those described above for HP0377, except that the elution buffer for size-exclusion chromatography was 20 m*M* Tris–HCl pH 7.9, 150 m*M* NaCl. Oxidized apocytochrome c_{553} (HP1227$_{\rm ox}$) was prepared by incubating the purified apocytochrome c_{553} with a 100-fold excess of oxidized glutathione for 1 h at 296 K. Excess glutathione was removed using the same buffer for size-exclusion chromatography as described above. To ensure full oxidation of HP0377, the oxidized HP0377 sample used in crystallization was treated with a 100-fold excess of oxidized glutathione and the excess glutathione was removed (HP0377$_{\rm ox}$). Reduced apocytochrome c_{553} (HP1227$_{\rm red}$) was prepared by incubating the purified apocytochrome c_{553} with a 100-fold excess of TCEP for 1 h at 296 K. Excess TCEP was removed using a HiLoad 16/60 Superdex 200 prep-grade column (GE Healthcare) which was previously equilibrated with 20 m*M* Tris–HCl pH 7.9, 150 m*M* NaCl. To ensure full reduction of HP0377 for the reductase assay, the reduced HP0377 sample used in crystallization was similarly treated with a 100-fold excess of TCEP (HP0377$_{\rm red}$) and the excess TCEP was removed.

Oxidized apocytochrome c_{553} in 20 m*M* Tris–HCl pH 7.9, 150 m*M* NaCl was incubated for 3 h at 296 K in the presence (or absence) of a twofold excess of HP0377$_{\rm red}$. After incubation for 3 h, the proteins were precipitated with trichloroacetic acid [final concentration 5%(*w*/*v*)], washed with ice-cold acetone and then resuspended in 40 µl of a reaction buffer consisting of 50 m*M* Tris–HCl pH 6.8, 2%(*w*/*v*) SDS, 10 m*M* 4-acetamido-4′-maleimidylstilbene-2,2′-disulfonic acid (AMS; Invitrogen Molecular Probes). The alkylation agent AMS

specifically reacts with the free thiol groups of the reduced protein, but not with the disulfide bonds of the oxidized protein. Since AMS modification increases the mass of the protein by ∼0.5 kDa per thiol group, this method enables protein isoforms with different numbers of reduced cysteines to be resolved. The oxidized and reduced forms of HP0377 as well as reduced apocytochrome c_{553} were similarly treated with AMS before SDS–PAGE under nonreducing conditions. AMS-treated protein samples were separated by 15%(*w*/*v*) nonreducing SDS–PAGE and were visualized by Coomassie staining.

2.6. Covalent complex formation between HP0377 C92A and HP0518

The reduced HP0377 C92A variant and HP0518 modified with 2-nitro-5-thiobenzoic acid (HP0518-NTB) were mixed in a 3:1 molar ratio in the absence of any redox reagent. The protein mixture was incubated at 296 K for 3 h. Complex formation between reduced HP0377 C92A and HP0518 was monitored by size-exclusion chromatography on a Superdex 200 10/300 GL column (GE Healthcare) and multi-angle light scattering on a Wyatt MiniDAWN TREOS MALS instrument. The elution buffer was 20 m*M* Tris–HCl pH 7.9, 150 m*M* NaCl. Complex formation was also analyzed by SDS–PAGE.

In addition, liquid chromatography/mass spectrometry (LC-MS) analysis of the isolated reduced HP0377 C92A–HP0518 complex was performed to verify the formation of a disulfide bond between them. For disulfide-bond identification, the protein sample was digested with trypsin without reduction and alkylation. The protein sample dissolved in 50 m*M* ammonium bicarbonate pH 8.0 was digested with trypsin (1:50 protease:protein ratio) by overnight incubation at 310 K. The resulting peptides were analyzed using one-dimensional liquid chromatography/tandem mass spectrometry (1D LC-MS/MS). Peptides were identified using MS/MS with a nano-LC-MS system consisting of a Nano Acquity UPLC system (Waters, USA), a linear ion trap and a Fourier transform (FT) ion cyclotron resonance (ICR) mass spectrometer (Thermo Scientific, USA) equipped with a nano-electrospray source. An autosampler was used to load 4 µl aliquots of the peptide solutions onto a C18 trap column (300 µm internal diameter, 5 mm length and 5 µm particle size; Waters). The peptides were desalted and concentrated on the column at a flow rate of 5 µl min^{-1}. Next, the trapped peptides were back-flushed and separated on a 100 mm home-made microcapillary column consisting of C18 (Aqua; 3 µm particle size) packed into 75 µm silica tubing with an orifice internal diameter of 6 µm. The mobile phases, *A* and *B*, were composed of 100% water and 100% acetonitrile, respectively, and each contained 0.1% formic acid. The LC gradient was started with 5% *B* for 5 min and was ramped to 15% *B* over 5 min, to 50% *B* over 75 min, to 95% *B* over 5 min and remained at 95% *B* for 5 min and 5% *B* for a further 5 min. The column was re-equilibrated with 5% *B* for 15 min before the next run. The voltage applied to produce an electrospray was 2.2 kV. In each duty circle of mass analysis, one high-resolution (1 in 100 000) mass spectrum was acquired using the FT-ICR analyzer, followed by five data-dependent MS/MS scans using the linear ion-trap analyzer. For MS/MS analysis, a normalized collision energy (35%) was used throughout the collision-induced dissociation phase. All MS/MS data were manually analyzed for peptide identification. To determine disulfide-linked sites, we took the fragmentation patterns of disulfide-linked peptides into account, considering fragment ions including cysteine, cysteine persulfide and dehydroalanine (Choi *et al.*, 2010).

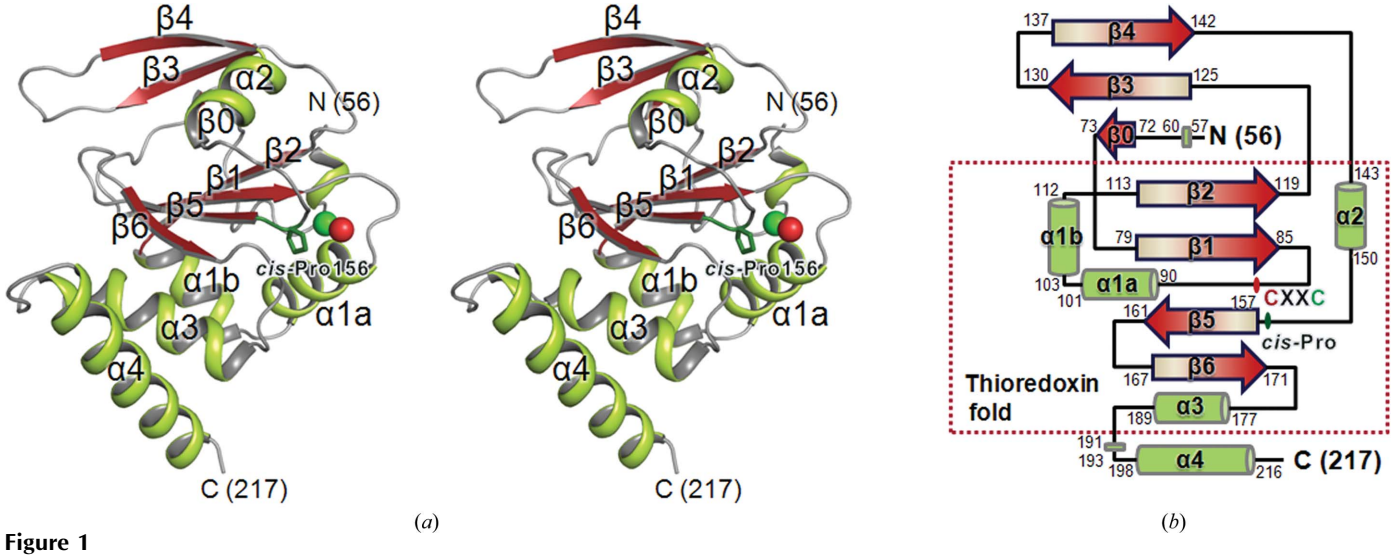

Figure 1
Overall monomer structure and topology of HP0377. (*a*) Stereoview of an HP0377 monomer in cartoon representation, with the secondary-structure elements labelled. α-Helices are depicted in green and β-strands in red. S atoms of Cys89 and Cys92 in the C*XX*C motif are shown as red and green spheres, respectively. The *cis*-Pro156 is shown as a green stick model. (*b*) A topology diagram of HP0377 (chain *B*, oxidized state) is shown with the same colour scheme as in (*a*). The classic thioredoxin fold is encircled by a red dotted box. Residue numbers for each secondary-structure element are indicated. α-Helices, 3_{10}-helices, β-strands and loops are shown as cylinders (green), flat cylinders (green), arrows (graded red) and solid lines, respectively. Structural figures were drawn using *PyMOL* (DeLano, 2002).

3. Results

3.1. Overall structure of HP0377

Crystal structures of HP0377 have been determined in both reduced and partially oxidized states using the 33–221 construct with an added N-terminal fusion tag. This construct excludes the predicted signal peptide (Met1–Ser23) and nine additional residues at the N-terminus. The two monomers of HP0377 in the asymmetric unit of the *C*2 unit cell are highly similar to each other, with root-mean-square deviations (r.m.s.d.s) of 0.45 Å for 161 C^{α} atoms in the reduced model and 0.53 Å for 160 C^{α} atoms in the partially oxidized model. The model of reduced HP0377 has been refined to crystallographic R_{work} and R_{free} values of 19.1 and 23.8%, respectively, for data with resolution 20.0–2.30 Å. It encompasses residues Asp56–Ser216. Leu33–Ile55 of both chains, Ser218–Asn221 of chain *A*, Lys217–Asn221 of chain *B* and the N-terminal fusion tag are disordered. The model of partially oxidized HP0377 has been refined to crystallographic R_{work} and R_{free} values of 19.5 and 23.0%, respectively, data with resolution 20.0–2.20 Å. In this model, the N-terminal regions (Leu33–Asn54 in chain *A* and Leu33–Ile55 in chain *B*) and the C-terminal regions (Ser216–Asn221 in chain *A* and Ser218–Asn221 in chain *B*) as well as the N-terminal fusion tag are disordered in the crystal. The two models of HP0377 are highly similar to each other, with r.m.s.d.s of 0.32–0.60 Å for pairwise comparisons of 160–162 C^{α} atoms. Large deviations between the two redox states are found in the loop connecting β-strands β3 and β4 (Asp132–Glu136), with a maximum C^{α} deviation of 3.8 Å at Asn134, and the region covering the C-terminal helix α4 and a preceding loop (Asp189–Leu215), with a maximum C^{α} deviation of 1.7 Å at Asp197. These two regions have higher *B* factors than average and are probably flexible. They are spatially well separated from the active site of HP0377 (Fig. 1*a*).

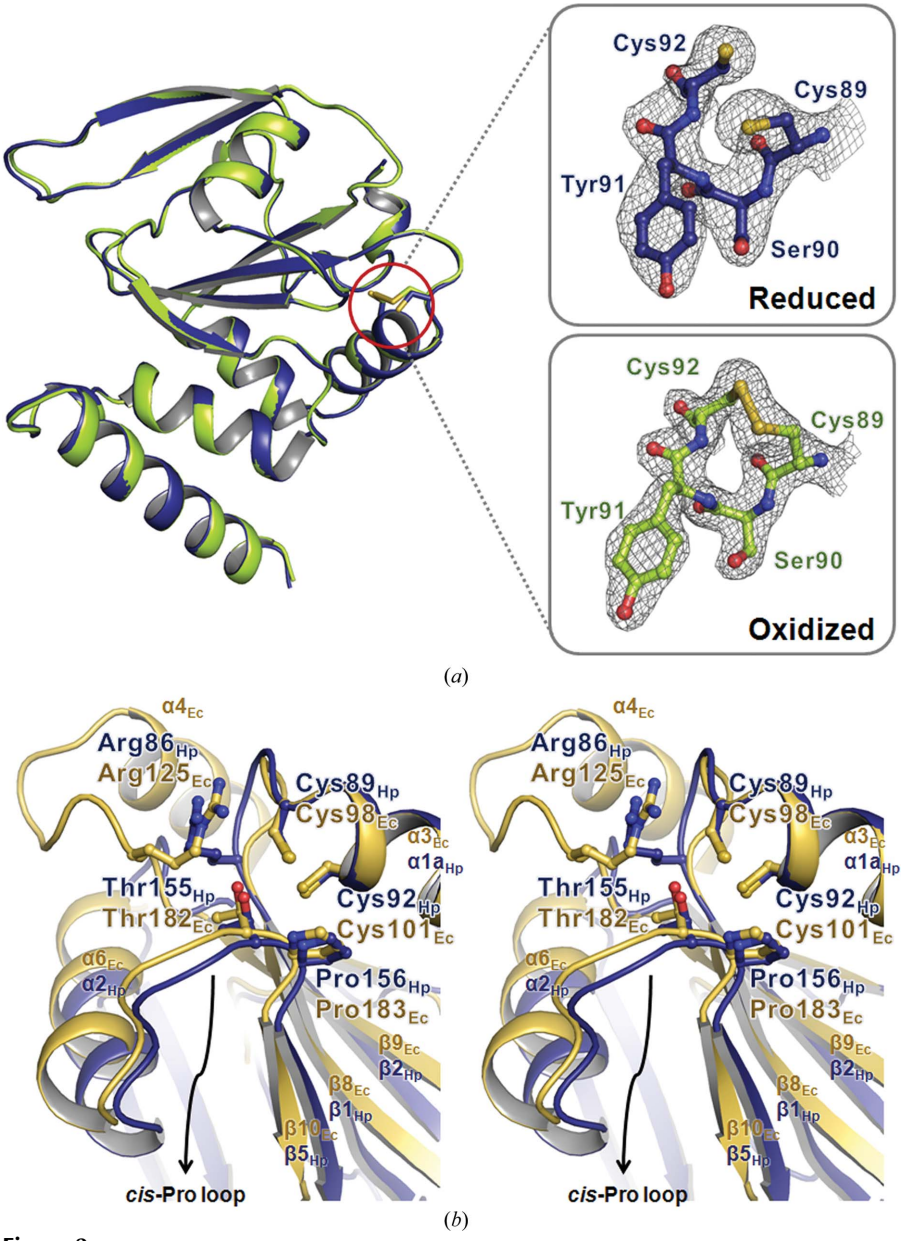

Figure 2
Structural comparisons of reduced HP0377 with partially oxidized HP0377 and reduced *E. coli* DsbC. (*a*) Monomers *A* of reduced HP0377 (blue) and partially oxidized HP0377 (green) models are superimposed (left), with the S atoms of Cys89 and Cys92 shown as stick models. On the right, the $2mF_o - DF_c$ electron-density maps (grey mesh) of reduced HP0377 (top) and partially oxidized HP0377 (bottom) are shown at the 1.5σ level around the active-site cysteine residues. (*b*) Stereoview of the active-site region after superimposing the C*XX*C motifs of reduced HP0377 and reduced *E. coli* DsbC. Catalytic cysteine residues and the structurally conserved Arg residue, as well as the *cis*-Pro residue and the residue preceding it, are shown as ball-and-stick models with labelling. Secondary-structure elements of both proteins are labelled.

In the model of reduced HP0377, the electron density around Cys89 and Cys92 clearly shows that they are fully reduced, with sulfur–sulfur distances of 3.63 and 3.44 Å for chains *A* and *B*, respectively (Fig. 2*a*). In the structure of chain *A* of oxidized HP0377, the electron density around the S atoms of Cys89 and Cys92 of the C*XX*C motif clearly indicates the presence of a disulfide bond but with partial cleavage (Fig. 2*a*). It is likely that the intense synchrotron X-rays caused partial cleavage of the disulfide bond during data collection. Similar disulfide cleavages by synchrotron radiation have been observed previously (Roberts *et al.*, 2005; Stirnimann *et al.*, 2006). When we modelled the disulfide bond in chain *A* of oxidized HP0377 with a single conformation, negative electron density remained between the two S atoms in

the $F_o - F_c$ map. The negative electron density disappeared when we modelled it as a mixture of fully oxidized and cleaved models with occupancies of 0.20 (S–S distance of 2.03 Å) and 0.80 (S–S distance of 2.80 Å). For chain *B*, the negative electron density between the S atoms disappeared when we lowered the occupancies of the S atoms to 0.9 (S–S distance of 2.14 Å). Sulfur–sulfur distances that were somewhat longer than the usual 2.0 Å for a disulfide bond but shorter than the usual 3.4 Å for fully reduced thiols were previously observed (Stirnimann *et al.*, 2006). In the structure of the C-terminal domain of *E. coli* DsbD (cDsbD; PDB entry 2fwh; TCEP-reduced at pH 7.0; Stirnimann *et al.*, 2006), the occupancies of the S atoms of Cys464 and Cys461 were lowered to 0.9 and 0.8 during refinement to remove negative electron density around the S atoms.

HP0377 has a classic thioredoxin fold composed of [β1–(α1a–α1b)–β2]–α2–(β5–β6–α3), with three major modifications. The modifications are the distinct insertion of a two-stranded β-sheet (β3 and β4) between β2 and α2, and extensions at both the N- and C-termini (3_{10}-helix η1 and β0; α4) (Fig. 1). Modifications of the classic thioredoxin fold have previously been reported (Martin, 1995). The central four-stranded β-sheet made up of $\beta2\uparrow\beta1\uparrow\beta5\downarrow\beta6\uparrow$ is covered by four helices (α1a, α1b, α3 and α4) on one side and by a three-stranded β-sheet ($\beta0\uparrow\beta3\uparrow\beta4\downarrow$) and the connecting helix α2 on the other. The two helices α1a and α1b of HP0377 are separated by Val102, whereas they are merged into a single helix in *E. coli* thioredoxin (Ren *et al.*, 2009). Among the conserved active-site features of thioredoxin-family proteins, the C*XX*C motif of HP0377 is located N-terminal to the first helix (α1a); it is positioned in close spatial proximity to the *cis*-Pro156 loop which lies immediately before strand β5 (Fig. 1).

3.2. A *DALI* search reveals unique structural features of HP0377

A *DALI* search (Holm & Rosenström, 2010) revealed that HP0377 shows structural similarity, with *Z*-scores of 7.0–9.0, to thioredoxin-fold proteins that are involved in cytochrome reduction. They include the *B. subtilis* thiol-disulfide oxidoreductase ResA (PDB entry 1st9; Crow *et al.*, 2004), the *E. coli* cytochrome *c* biogenesis protein CcmG (PDB entry 2b1k; Ouyang *et al.*, 2006), the *B. japonicum* cytochrome *c* biogenesis protein CcmG (PDB entry 1kng; Edeling *et al.*, 2002) and the *B. japonicum* thiol-disulfide interchange protein TlpA (PDB entry 1jfu; Capitani *et al.*, 2001). Interestingly, these proteins have an insertion of an α-helix and a β-strand at the same location between β2 and α2 of the classic thioredoxin fold as in HP0377 (Supplementary Fig. S1). They also have an extension at the N-terminus, whereas they lack an extension at the C-terminus (Supplementary Fig. S1). In *B. japonicum* TlpA, Cys10 of α1 at the N-terminus forms a disulfide bridge to Cys155 positioned just before β8 and this unique disulfide bridge in *B. japonicum* TlpA serves the structural function of anchoring a long N-terminal extension to the remainder of the protein (Capitani *et al.*, 2001). It has been reported that the additional regions (one β-hairpin at the N-terminus and a central insertion comprising an α-helix and a β-strand) to the thioredoxin fold are essential for cytochrome *c* maturation in *E. coli* CcmG (Ouyang *et al.*, 2006; Edeling *et al.*, 2002, 2004). The deletion of an N-terminal β-sheet (57 residues in total) in *E. coli* CcmG causes remarkable changes in secondary structure and cannot complement cytochrome *c* maturation, suggesting that this region is essential for stabilizing the active-site structure for activity (Ouyang *et al.*, 2006; Edeling *et al.*, 2004). The central insertion of *E. coli* CcmG, which is adjacent to the C*XX*C active site and is highly conserved in the CcmG homologues, is also important for cytochrome *c* formation (Edeling *et al.*, 2002). The distinctive structural features of HP0377 could possibly affect its interactions with its partner protein(s). However, further studies are necessary to establish the functional roles of the additional regions of HP0377. Further discussions on structurally similar proteins as well as proteins with the insertion between β2 and α2 of the classic thioredoxin fold and an extension at the C-terminus are given in §2.1 of the Supplementary Material (Supplementary Figs. S2 and S3).

3.3. HP0377 exists as monomers in solution

Because the oligomeric state of HP0377 could be important in its function, we carried out a sedimentation-equilibrium ultracentrifugation analysis with the 33–221 construct at three different protein concentrations (7.7, 10.4 and 12.9 μM) in the presence of TCEP. A representative result measured at 20 000 rev min^{-1} using a 10.4 μM protein sample is presented in Supplementary Fig. S4(*a*). All of the measured data can be fitted well to a monomer model, with the distributions of residuals being random. To investigate the potential effect of the altered N-terminus on the oligomeric state, we also tested the 24–221 construct and confirmed that it is also monomeric in the presence of TCEP. A representative result for HP0377 (24–221) measured at 24 000 rev min^{-1} using a protein concentration of 10.3 μM is presented in Supplementary Fig. S4(*b*). These results indicate that functional HP0377 lacking the signal peptide is likely to exist as monomers in solution under reducing conditions. However, we do not rule out the possibility that disulfide-linked dimers of HP0377 can be formed through Cys25 in the case of HP0377 (24–221), although the physiological significance of such disulfide-linked dimers is unclear. Therefore, the oligomeric state of HP0377 is more similar to monomeric periplasmic thioredoxin-like proteins than to *E. coli* DsbC and *H. influenzae* DsbC, both of which are dimeric. The monomeric periplasmic thioredoxin-like proteins include *B. subtilis* ResA, *E. coli* CcmG, *B. japonicum* CcmG and *B. japonicum* TlpA. They contain a classic thioredoxin fold with some insertions and extensions. This result in solution is also consistent with our crystal structure, which did not reveal a tightly associated dimeric unit. The buried surface area in the interface between two HP0377 monomers that make the most extensive contacts with each other in the crystal is 440 Å^2 per monomer, as calculated using *PISA* (Krissinel & Henrick, 2007). This value is considerably smaller than those for the dimeric DsbC proteins

from *E. coli* and *H. influenzae*. The buried surface areas are 860 and 790 Å^2 per monomer for *E. coli* DsbC (PDB entry 1eej; McCarthy *et al.*, 2000) and *H. influenzae* DsbC (PDB entry 1t3b; Zhang *et al.*, 2004), respectively.

We hypothesize that monomeric HP0377 is more suitable for carrying out functions similar to monomeric periplasmic thioredoxin-like proteins such as *B. subtilis* ResA, *E. coli* CcmG and *B. japonicum* CcmG, which are involved in cytochrome *c* biogenesis (Erlendsson *et al.*, 2003; Fabianek *et al.*, 1997, 1998) and *B. japonicum* TlpA, which is involved in cytochrome aa_3 biogenesis and is speculated to keep the cysteines of the Cu_A binding site in subunit II of the aa_3-type oxidase reduced for incorporation of the copper cofactor (Loferer *et al.*, 1995). However, we do not rule out the possibility that the monomeric HP0377 can serve a similar function to dimeric DsbC proteins.

3.4. HP0377 may be involved in cytochrome *c* biogenesis

The *hp0377* gene is located just upstream of the *hp0378* gene and is flanked by the *hp0378* gene in the same operon (Sharma *et al.*, 2010). The *hp0378* gene, a single large ORF that is a natural fusion of the *ccsB* and *ccsA* genes, encodes the CcsBA protein (Frawley & Kranz, 2009; Goddard *et al.*, 2010). The *H. pylori* CcsBA protein functions as a minimal haem-delivery system that also exhibits haem lyase activity (Hamel *et al.*, 2009; Feissner *et al.*, 2006). In addition, the HP0377 protein shows 15% overall sequence identity to *B. subtilis* ResA. In light of the similar gene structures and detectable sequence homology between HP0377 and *B. subtilis* ResA, we performed experiments to investigate whether HP0377 functions as a component of system II cytochrome *c* biogenesis. Specifically, we tested whether reduced HP0377 can reduce the cysteines in the C*XX*CH motif of apocytochrome *c*, which is a prerequisite for haem attachment.

It has been reported that cytochrome c_{553} is the only *c*-type cytochrome in the soluble fraction of the *H. pylori* NCTC 11637 culture (Koyanagi *et al.*, 2000). Holocytochrome c_{553} purified from the culture of *H. pylori* NCTC 11637 gave an α absorption-band peak at 553 nm in its reduced state (Koyanagi *et al.*, 2000). Thus, for testing the *in vitro* redox reaction, we chose HP1227 (annotated as cytochrome c_{553}) among the five predicted *c*-type cytochromes in *H. pylori* (HP0145, HP0147, HP1227, HP1461 and HP1538; Goldman & Kranz, 1998). We have expressed and purified the mature form (residues 20–96) of HP1227 in *E. coli* with a C-terminal fusion tag, since HP1227 contains a signal peptide (residues 1–19). Its sole cysteine residues, Cys29 and Cys32, belong to the haem-binding C*XX*CH motif. We confirmed that the purified *H. pylori* apocytochrome c_{553} is in the apo form by ESI-MS (the calculated mass of the apoprotein including the C-terminal fusion tag is 9437 Da; the observed mass is 9434 Da) and by recording visible absorption spectra, in which the characteristic bands of holocytochrome c_{553} were absent at 410 and 526 nm for the oxidized state and at 418, 524 and 553 nm for the reduced state (Koyanagi *et al.*, 2000).

We tested whether the reduced HP0377 can catalyze the reduction of oxidized apocytochrome c_{553} using the AMS alkylation method (Vestweber & Schatz, 1988; Uchida *et al.*, 1995), which is used to determine the redox states of cysteine-containing proteins (Kobayashi *et al.*, 1997). When we incubated oxidized apocytochrome c_{553} with reduced HP0377, we observed the conversion of oxidized apocytochrome c_{553} to the reduced form (Fig. 3*a*, lane 3) as well as the conversion of reduced HP0377 to the oxidized form (Fig. 3*b*, lane 3′). In the absence of HP0377, oxidized apocytochrome c_{553} was not converted to the reduced form (Fig. 3*a*, lane 2). These results suggest that HP0377 may be involved in cytochrome *c* biosynthesis in *H. pylori* by reducing the haem-binding C*XX*CH motif of apocytochrome c_{553} prior to the haem-ligation reaction.

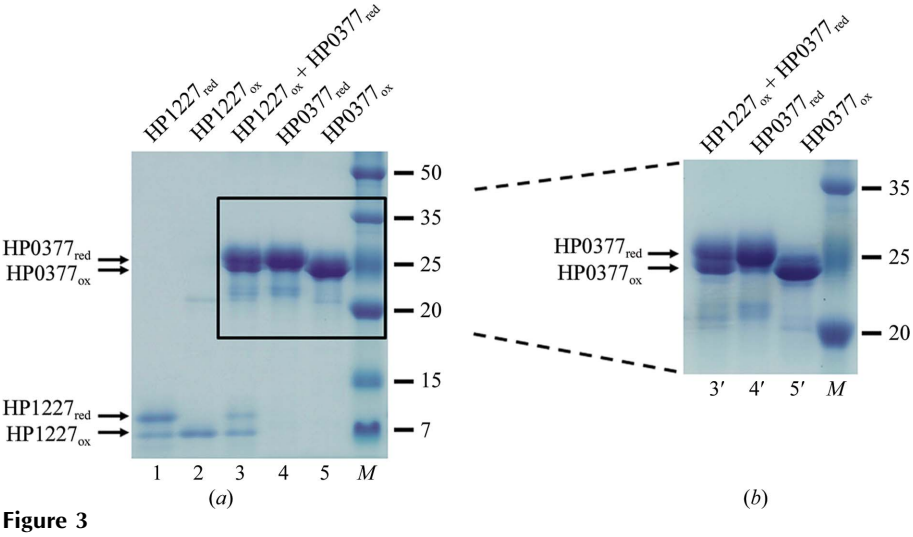

Figure 3
Reduction assay of HP0377 towards apocytochrome c_{553} (HP1227) from *H. pylori*. (*a*) HP0377-dependent reduction of oxidized apocytochrome c_{553}. Lane 1, reduced apocytochrome c_{553}. Lane 2, oxidized apocytochrome c_{553}. Lane 3, oxidized apocytochrome c_{553} (10 µ*M*) treated with reduced HP0377 (20 µ*M*). Lane 4, reduced HP0377. Lane 5, oxidized HP0377. Lane *M*, prestained protein ladder (labelled in kDa). Different redox forms were detected by nonreducing SDS–PAGE after AMS treatment, which results in an increase in the molecular mass of alkylated proteins by about 0.5 kDa per thiol group. The gel was run for 40 min. (*b*) In a separate experiment, another gel was run for 80 min to better resolve reduced HP0377 and oxidized HP0377. Lanes 3′ to 5′ are the same as lanes 3 to 5 in (*a*). Lane *M*, the same prestained protein ladder as in (*a*).

3.5. HP0377 forms a covalent complex with HP0518

It has been reported that the dimeric *E. coli* DsbC can serve as a backup for *E. coli* DsbG, which protects the catalytic cysteine residue of YbiS, the most active L,D-transpeptidase in the periplasm, from oxidation (Depuydt *et al.*, 2009). HP0377 is highly divergent in sequence from *E. coli* DsbC, with only 12% sequence identity. Furthermore, HP0377 is monomeric in solution and is also highly divergent from *E. coli* DsbC

in tertiary structure. However, the two proteins share similar active-site structures, as discussed in detail below. This suggests that HP0377 could possibly function as a reductase towards a catalytic cysteine-containing L,D-transpeptidase in a manner similar to *E. coli* DsbC.

Therefore, we tested whether HP0377 can reduce *H. pylori* HP0518, which contains a conserved single cysteine residue (Cys176) in its putative L,D-transpeptidase domain. The corresponding conserved cysteine residues of L,D-transpeptidases from *B. subtilis* (Cys139) and *Enterococcus faecium* (Cys442) were shown to be catalytically important and need to be kept in the reduced state for catalytic activity (Bielnicki *et al.*, 2006; Biarrotte-Sorin *et al.*, 2006). We performed a reductase assay using DTNB-treated HP0518 as a potential substrate and monitored the reaction by the absorbance of the released anion (NTB^{2-}) at 412 nm. HP0377 showed reductase activity towards HP0518, a putative L,D-transpeptidase, but the reaction between HP0377 and HP0518 was slower than with *H. pylori* DsbG (HP0231; Supplementary Fig. S5).

In order to trap a stable disulfide-bonded intermediate between HP0377 and HP0518 for further characterization, we mutated the second active-site cysteine (Cys92) of HP0377 to alanine and modified the single cysteine (Cys176) of HP0518 using DTNB. An excess of the fully reduced HP0377 C92A variant was mixed with HP0518-NTB in a molar ratio of 3:1 owing to the absence of a recycling redox system in the reaction tube. After 3 h of incubation, size-exclusion chromatography was performed and the peak corresponding to a possible covalent complex between the reduced HP0377 C92A variant and HP0518-NTB was assessed by multi-angle light scattering to determine the approximate molecular mass (Supplementary Fig. S6*a*). Coomassie-stained SDS–PAGE of this peak confirmed the presence of both HP0377 and HP0518 in a roughly 1:1 molar ratio (Supplementary Fig. S6*b*, lane 3). The molecular masses of the complex, the reduced HP0377 C92A variant and HP0518 (fused with a 21-residue N-terminal tag) were estimated by multi-angle light scattering to be 148 ± 20, 32 ± 4 and 82 ± 3 kDa, respectively. They agree with the theoretical masses of 127.1, 24.0 and 79.2 kDa, respectively, for a 2:2 complex between reduced HP0377 C92A and HP0518, monomeric HP0377 C92A variant and dimeric HP0518. When an equimolar amount of the reduced HP0377 C92A variant was mixed with HP0518-NTB, SDS–PAGE of the isolated complex showed reduced intensity for HP0377, suggesting the possibility of forming a 1:2 complex between a monomer of HP0377 and a dimer of HP0518 (Supplementary Fig. S7, lane 1).

Furthermore, we confirmed the formation of the covalent complex by MS/MS analysis of a disulfide-bonded pair of peptides isolated from the reduced HP0377 C92A–HP0518 complex after tryptic digestion (Supplementary Fig. S8). Fragments denoted y_n (n = 3–9) were generated from the C-terminus of the Cys176-containing peptide of HP0518, whereas fragments denoted b_n+P2 ($n = 2-14$) were produced from the disulfide-bonded pair of peptides between the N-terminal fragments of the Cys176-containing peptide of HP0518 and the Cys89-containing peptide of HP0377. This result indicates that the expected disulfide linkage between Cys89 of HP0377 and Cys176 of HP0518 is made when the reduced HP0377 C92A variant and HP0518 interact with each other. Taken together, these results suggest that HP0377 could function as a reductase towards HP0518 as well as apocytochrome c_{553}.

3.6. Active-site features of HP0377

The C*XX*C motif and the *cis*-Pro loop are the conserved active-site features among the redox-active proteins of the thioredoxin fold and are important in the activity, substrate recognition and stabilization of these proteins (Quan *et al.*, 2007; Lafaye *et al.*, 2009). The C*XX*C motif of HP0377 is located at the N-terminus of the first helix (α1a; Figs. 1 and 2*b*). In both reduced and partially oxidized states of HP0377 Cys89 is exposed to the bulk solvent, whereas Cys92 is buried. Cys89 is more exposed to the solvent in the reduced state, with the S atoms of Cys89 being 0.58–1.08 Å apart in the two redox states. This indicates that the more exposed Cys89 in the reduced state is poised for nucleophilic attack on the disulfide bond of its substrate(s). The side chain of Cys89 in the reduced state interacts with the backbone amide and the side chain of Cys92, the hydroxyl group of Thr155 and the guanidinium group of Arg86 as well as a positive charge from the helix dipole of α1a (Fig. 2*b*). Interestingly, the side chain of Cys89 of HP0377 in the reduced state points in the opposite direction to that of the corresponding cysteine residue (Cys74) of *B. subtilis* ResA in the reduced state (Supplementary Fig. S9).

Cys74 of *B. subtilis* ResA in the reduced state is partly shielded from solvent by the hydrophobic side chains of Trp73 and Leu140 (Crow *et al.*, 2004). It has been suggested that partial shielding of Cys74 may confer protection against protein inactivation and nonspecific electron transfer (Crow *et al.*, 2004). In HP0377, the corresponding residues to Trp73 and Leu140 in *B. subtilis* ResA are Gly88 and Thr155, respectively, and no such shielding of Cys89 by an aromatic ring is observed (Supplementary Fig. S9). This suggests that the substrate specificity of HP0377 may be broader than that of *B. subtilis* ResA. The two internal residues of the C*XX*C motif of thiol-disulfide oxidoreductases have been reported to be the major determinants in modulating their redox properties (Huber-Wunderlich & Glockshuber, 1998). The catalytic C*XX*C motif of HP0377 is composed of Gly-Cys-Ser-Tyr-Cys, whereas the *B. subtilis* ResA and CcmG homologues contain the active-site motif Trp-Cys-Xxx-Xxx-Cys. The central dipeptide sequence (Ser-Tyr) in the C*XX*C motif of HP0377 is more similar to DsbC homologues, which often have Xxx-Tyr in the corresponding region (Ren *et al.*, 2009). The central dipeptide sequences in *B. subtilis* ResA and CcmG homologues are variable.

An arginine residue (Arg125) of *E. coli* DsbC on the loop between β9 and α4 is positioned near the characteristic C*XX*C motif by extensive hydrogen-bonding networks (McCarthy *et al.*, 2000), and specific hydrogen-bond interactions stabilize the active site in the reduced state of *E. coli* DsbC (Banaszak *et al.*, 2004; Fig. 2*b*). This arginine residue is conserved in the

sequences of other DsbC homologues. In *H. influenza* DsbC, the corresponding residue, Arg125, is positioned at an essentially identical location and appears to play the same role (Zhang *et al.*, 2004). When the reduced model of HP0377 is superimposed on the thioredoxin domain of reduced *E. coli* DsbC (PDB entry 1tjd), the loop between β9 and α4 of *E. coli* DsbC is highly truncated in HP0377 (Fig. 2*b*). However, Arg86 on the loop between β1 and α1a is located in a nearly identical position in HP0377 (Fig. 2*b*). This suggests that Arg86 of HP0377 may influence the active-site Cys89 in a manner similar to the conserved arginine residue (Arg125) in the *E. coli* and *H. influenzae* DsbCs. To gain insight into the role of Arg86, we substituted Arg86 with alanine and compared the insulin reductase activity (Supplementary Fig. S10), redox potential (Supplementary Fig. S11*a*) and the pK_a of the nucleophilic cysteine Cys89 (Supplementary Fig. S11*b*), as well as the thermostability of the wild type and the R86A mutant (Supplementary Table S1). The results indicate that Arg86 plays a minor role as one of the factors that control the stability and redox properties of HP0377.

The second active-site feature among the redox-active proteins of the thioredoxin fold is the so-called *cis*-Pro loop, which is located between α2 and β5 of HP0377. The *cis*-Pro loop is spatially positioned adjacent to the C*XX*C motif and has been shown to be important in substrate recognition by redox-active proteins of the thioredoxin fold (Kadokura *et al.*, 2004). Superposition of the reduced HP0377 model with the reduced structure of *E. coli* DsbC reveals that their *cis*-Pro loops are highly similar in length and conformation (Fig. 2*b* and Supplementary Fig. S12), despite the fact that the loop between β9 and α4 of *E. coli* DsbC is highly truncated in HP0377 (Fig. 2*b*). Both proteins also have a threonine residue preceding the *cis*-Pro residue (Fig. 2*b*). This feature is conserved among DsbC homologues (Ren *et al.*, 2009). In contrast, the corresponding residue is hydrophobic in *B. subtilis* ResA and the CcmG homologues from *B. japonicum* and *E. coli* (Leu140, Val156 and Ala143, respectively). The residue preceding *cis*-Pro appears to control the activity of thioredoxin-family proteins by affecting both their redox properties and their ability to interact with partner proteins (Ren *et al.*, 2009). These common structural features are consistent with our finding that HP0377 forms a covalent complex with HP0518 *via* an expected disulfide bond (as discussed in §3.5 above) in order to function as a DsbC-like reductase. However, neither the presence of a Tyr in the C*XX*C motif nor the presence of a Thr preceding the *cis*-Pro is a conclusive piece of evidence for a DsbC-like reductase function because both of these motifs are found in *Staphylococcus aureus* DsbA (Heras *et al.*, 2008).

Interestingly, we observed extra electron density at the protein surface in close proximity to the active-site Cys89 in chain *A* of the reduced HP0377 model (Supplementary Fig. S13). We modelled it as a PEG molecule of 194 Da (Supplementary Fig. S13) which appears to be a contaminant of the precipitant (PEG 3350). The cleft in which the PEG molecule is bound is formed by α1, the α2–β5 loop and the β6–α3 loop. It is lined with hydrophobic residues (Tyr91, Pro156, Leu171, Pro172, Gly173, Tyr174, Met175 and Pro176). The modelled PEG interacts with the main-chain N atoms of Thr155 and Tyr174 and also with the hydrophobic side chains of Tyr91, Tyr174 and Met175. A similar cleft is present in chain *B* of the reduced HP0377 model as well as in both chains *A* and *B* of the partially oxidized HP0377 model, but is not occupied by PEG. The observed binding of a PEG molecule near the active site of HP0377 may provide insight into the substrate binding in the active site.

4. Discussion

c-type cytochromes function in a range of redox reactions in bacteria. Cytochrome c_{553} (HP1227) from *H. pylori* has been identified as a potential electron donor to the *cb*-type cytochrome *c* oxidase (Tsukita *et al.*, 1999). *H. pylori* utilizes the system II pathway for the synthesis of cytochrome *c*. Before covalent attachment of the haem group, the active-site cysteines of apocytochrome c_{553} must be kept reduced by a component of the *H. pylori* system II. In this study, we suggest that HP0377 may function as a reductase towards *H. pylori* apocytochrome c_{553} (HP1227; Fig. 3). Our result supports the role of HP0377 as a component of the *H. pylori* system II for cytochrome *c* maturation. In the genome of *H. pylori* 26695 the *hp0377* gene is located between *hemH* (*hp0376*), a gene for haem biosynthesis, and *ccsBA* (*hp0378*), a gene for haem export and the attachment of haem to apocytochrome *c* (Frawley & Kranz, 2009). Moreover, the *hp0377* gene exists with the *hp0378* gene in a single operon (Sharma *et al.*, 2010). A similar gene structure is found in *B. subtilis*, which also adopts the system II pathway for cytochrome *c* biogenesis. *B. subtilis* ResA, which shows 15% overall sequence identity to HP0377, has specificity for apocytochromes *c* (Colbert *et al.*, 2006).

Moreover, the remarkable structural similarity between the active sites of HP0377 and *E. coli* DsbC prompted us to investigate the possibility that HP0377 may function as a reductase like *E. coli* DsbC, which plays a role as a backup for DsbG in protecting the catalytic cysteine of the YbiS L,D-transpeptidase from oxidation (Depuydt *et al.*, 2009). We have shown that HP0377 can reduce HP0518, a putative L,D-transpeptidase from *H. pylori*, and form a covalent complex *via* the expected disulfide bond (Supplementary Figs. S5, S6 and S8). Taken together, these results suggest that HP0377 has a broader substrate specificity than *B. subtilis* ResA, which is a component of the system II pathway for cytochrome *c* biogenesis.

Large structural differences are observed between the two redox states of *B. subtilis* ResA around the active site. That is, part of the β3–α1 loop and α1 (Trp73–Lys79) and the β7–α4 loop (Gly158–Met160) show relatively large conformational changes, with maximum C^{α} deviations of 3.6 Å at Cys77 and 6.3 Å at Gly158, respectively. *B. subtilis* ResA appears to use its altered surface features to recognize the substrate in a specific orientation (Crow *et al.*, 2004; Colbert *et al.*, 2006). The region near the active site of *B. subtilis* ResA is relatively hydrophobic in the oxidized state, whereas it becomes more

basic upon reduction (Crow *et al.*, 2004). In addition, the cavity in the vicinity of the active site is only formed in the reduced state of *B. subtilis* ResA and seems to be suitable for recognizing the histidine residue of the C*XX*CH motif of apocytochromes (Lewin *et al.*, 2006). Such a 'histidine-clamp' mechanism would confer specificity for recognition of apocytochrome *c* (Crow *et al.*, 2004).

The redox-coupled conformational changes of *B. subtilis* ResA have been proposed as a general feature of the thiol reductases involved in cytochrome *c* maturation (Crow *et al.*, 2004), because the residues involved in redox-coupled conformational changes in *B. subtilis* ResA (Asn68, Pro76, Glu80, Pro141, Gly158 and Thr159) are well conserved in many CCM-related apocytochrome reductases. Moreover, structural comparisons of oxidized *B. subtilis* ResA with oxidized forms of *E. coli* CcmG, *B. japonicum* CcmG and *B. japonicum* TlpA show that these regions are very similar (Crow *et al.*, 2004). However, structural superpositions indicate that the residues proposed above to be involved in redox-coupled conformational changes are not well conserved in HP0377 (Val83, Tyr91, Phe95, Pro156, Gly173 and Tyr174); therefore, we suspect that HP0377 may employ a different mode of recognizing apocytochrome *c*. Similarly to HP0377, *E. coli* cDsbD and *E. coli* thioredoxin have been reported to undergo hardly any conformational change upon disulfide reduction (Stirnimann *et al.*, 2006; Jeng *et al.*, 1994). Our structural and functional characterizations of HP0377, together with the small genome size of *H. pylori* (1.67 Mbp) compared with *B. subtilis* (4.17 Mbp), suggest the possibility that HP0377 has evolved to serve multiple functions as a reductase in *H. pylori*.

We thank the beamline staff at the Pohang Light Source, Korea (BL-4A and BL-6C) and the Photon Factory, Japan (BL-1A and BL-5A) for assistance during X-ray diffraction experiments. We also thank Professor Hyun Kyu Song of Korea University for technical support. This work was supported by the Korea Ministry of Education, Science and Technology, the National Research Foundation (NRF) of Korea, the Innovative Drug Research Center for Metabolic and Inflammatory Disease (grant No. R11-2007-107-00000-0), the Basic Science Outstanding Scholars Program, the World-Class University Program and the Korea Healthcare Technology R&D Project, Ministry of Health, Welfare and Family Affairs, Republic of Korea (grant No. A092006). This research was also supported by the NRF grant funded by the Korean government (2011-0013663) to HJY and by PAL through the Abroad Beamtime program of the Synchrotron Radiation Facility Project under MEST and has been performed under the approval of the Photon Factory Program Advisory Committee (Proposal No. 2010G704).

References

Achard, M. E., Hamilton, A. J., Dankowski, T., Heras, B., Schembri, M. S., Edwards, J. L., Jennings, M. P. & McEwan, A. G. (2009). *Infect. Immun.* **77**, 4934–4939.
Adams, P. D. *et al.* (2010). *Acta Cryst.* D**66**, 213–221.
Banaszak, K., Mechin, I., Frost, G. & Rypniewski, W. (2004). *Acta Cryst.* D**60**, 1747–1752.
Barker, P. D. & Ferguson, S. J. (1999). *Structure Fold. Des.* **7**, R281–R290.
Beckett, C. S., Loughman, J. A., Karberg, K. A., Donato, G. M., Goldman, W. E. & Kranz, R. G. (2000). *Mol. Microbiol.* **38**, 465–481.
Beckman, D. L. & Kranz, R. G. (1993). *Proc. Natl Acad. Sci. USA*, **90**, 2179–2183.
Biarrotte-Sorin, S., Hugonnet, J.-E., Delfosse, V., Mainardi, J.-L., Gutmann, L., Arthur, M. & Mayer, C. (2006). *J. Mol. Biol.* **359**, 533–538.
Bielnicki, J., Devedjiev, Y., Derewenda, U., Dauter, Z., Joachimiak, A. & Derewenda, Z. S. (2006). *Proteins*, **62**, 144–151.
Brünger, A. T. (1992). *Nature (London)*, **355**, 472–475.
Capitani, G., Rossmann, R., Sargent, D. F., Grütter, M. G., Richmond, T. J. & Hennecke, H. (2001). *J. Mol. Biol.* **311**, 1037–1048.
Chen, V. B., Arendall, W. B., Headd, J. J., Keedy, D. A., Immormino, R. M., Kapral, G. J., Murray, L. W., Richardson, J. S. & Richardson, D. C. (2010). *Acta Cryst.* D**66**, 12–21.
Choi, S., Jeong, J., Na, S., Lee, H. S., Kim, H.-Y., Lee, K.-J. & Paek, E. (2010). *J. Proteome Res.* **9**, 626–635.
Colbert, C. L., Wu, Q., Erbel, P. J., Gardner, K. H. & Deisenhofer, J. (2006). *Proc. Natl Acad. Sci. USA*, **103**, 4410–4415.
Crow, A., Acheson, R. M., Le Brun, N. E. & Oubrie, A. (2004). *J. Biol. Chem.* **279**, 23654–23660.
DeLano, W. L. (2002). *PyMOL*. http://www.pymol.org.
Depuydt, M., Leonard, S. E., Vertommen, D., Denoncin, K., Morsomme, P., Wahni, K., Messens, J., Carroll, K. S. & Collet, J.-F. (2009). *Science*, **326**, 1109–1111.
Deshmukh, M., Brasseur, G. & Daldal, F. (2000). *Mol. Microbiol.* **35**, 123–138.
Dumont, M. E., Ernst, J. F., Hampsey, D. M. & Sherman, F. (1987). *EMBO J.* **6**, 235–241.
Edeling, M. A., Ahuja, U., Heras, B., Thöny-Meyer, L. & Martin, J. L. (2004). *J. Bacteriol.* **186**, 4030–4033.
Edeling, M. A., Guddat, L. W., Fabianek, R. A., Thöny-Meyer, L. & Martin, J. L. (2002). *Structure*, **10**, 973–979.
Emsley, P. & Cowtan, K. (2004). *Acta Cryst.* D**60**, 2126–2132.
Epp, O., Ladenstein, R. & Wendel, A. (1983). *Eur. J. Biochem.* **133**, 51–69.
Erlendsson, L. S., Acheson, R. M., Hederstedt, L. & Le Brun, N. E. (2003). *J. Biol. Chem.* **278**, 17852–17858.
Fabianek, R. A., Hennecke, H. & Thöny-Meyer, L. (1998). *J. Bacteriol.* **180**, 1947–1950.
Fabianek, R. A., Huber-Wunderlich, M., Glockshuber, R., Künzler, P., Hennecke, H. & Thöny-Meyer, L. (1997). *J. Biol. Chem.* **272**, 4467–4473.
Feissner, R. E., Richard-Fogal, C. L., Frawley, E. R., Loughman, J. A., Earley, K. W. & Kranz, R. G. (2006). *Mol. Microbiol.* **60**, 563–577.
Ferguson, S. J., Stevens, J. M., Allen, J. W. & Robertson, I. B. (2008). *Biochim. Biophys. Acta*, **1777**, 980–984.
Foloppe, N. & Nilsson, L. (2007). *J. Mol. Biol.* **372**, 798–816.
Frawley, E. R. & Kranz, R. G. (2009). *Proc. Natl Acad. Sci. USA*, **106**, 10201–10206.
Giegé, P., Grienenberger, J. M. & Bonnard, G. (2008). *Mitochondrion*, **8**, 61–73.
Goddard, A. D., Stevens, J. M., Rondelet, A., Nomerotskaia, E., Allen, J. W. & Ferguson, S. J. (2010). *FEBS J.* **277**, 726–737.
Goldman, B. S. & Kranz, R. G. (1998). *Mol. Microbiol.* **27**, 871–873.
Goulding, C. W., Apostol, M. I., Gleiter, S., Parseghian, A., Bardwell, J., Gennaro, M. & Eisenberg, D. (2004). *J. Biol. Chem.* **279**, 3516–3524.
Hamel, P., Corvest, V., Giegé, P. & Bonnard, G. (2009). *Biochim. Biophys. Acta*, **1793**, 125–138.
Heras, B., Kurz, M., Jarrott, R., Shouldice, S. R., Frei, P., Robin, G., Cemazar, M., Thöny-Meyer, L., Glockshuber, R. & Martin, J. L. (2008). *J. Biol. Chem.* **283**, 4261–4271.

Holm, L. & Rosenström, P. (2010). *Nucleic Acids Res.* **38**, W545–W549.
Holmgren, A. (1979). *J. Biol. Chem.* **254**, 3664–3671.
Huber-Wunderlich, M. & Glockshuber, R. (1998). *Fold. Des.* **3**, 161–171.
Jacobi, A., Huber-Wunderlich, M., Hennecke, J. & Glockshuber, R. (1997). *J. Biol. Chem.* **272**, 21692–21699.
Jeng, M. F., Campbell, A. P., Begley, T., Holmgren, A., Case, D. A., Wright, P. E. & Dyson, H. J. (1994). *Structure*, **2**, 853–868.
Kaakoush, N. O., Kovach, Z. & Mendz, G. L. (2007). *FEMS Immunol. Med. Microbiol.* **50**, 177–183.
Kadokura, H., Tian, H., Zander, T., Bardwell, J. C. & Beckwith, J. (2004). *Science*, **303**, 534–537.
Knott, G. D. (1979). *Math. Prog. Biom.* **10**, 271–280.
Kobayashi, T., Kishigami, S., Sone, M., Inokuchi, H., Mogi, T. & Ito, K. (1997). *Proc. Natl Acad. Sci. USA*, **94**, 11857–11862.
Koyanagi, S., Nagata, K., Tamura, T., Tsukita, S. & Sone, N. (2000). *J. Biochem.* **128**, 371–375.
Kranz, R., Lill, R., Goldman, B., Bonnard, G. & Merchant, S. (1998). *Mol. Microbiol.* **29**, 383–396.
Kranz, R. G., Richard-Fogal, C., Taylor, J. S. & Frawley, E. R. (2009). *Microbiol. Mol. Biol. Rev.* **73**, 510–528.
Krissinel, E. & Henrick, K. (2007). *J. Mol. Biol.* **372**, 774–797.
Ladbury, J. E., Kishore, N., Hellinga, H. W., Wynn, R. & Sturtevant, J. M. (1994). *Biochemistry*, **33**, 3688–3692.
Lafaye, C., Iwema, T., Carpentier, P., Jullian-Binard, C., Kroll, J. S., Collet, J.-F. & Serre, L. (2009). *J. Mol. Biol.* **392**, 952–966.
Laue, T. M., Shah, B. D., Ridgeway, T. M. & Pelletier, S. L. (1992). *Analytical Ultracentrifugation in Biochemistry and Polymer Science*, edited by S. E. Harding, A. J. Rowe & J. C. Horton, pp. 90–125. Cambridge: The Royal Society of Chemistry.
Lewin, A., Crow, A., Hodson, C. T., Hederstedt, L. & Le Brun, N. E. (2008). *Biochem. J.* **414**, 81–91.
Lewin, A., Crow, A., Oubrie, A. & Le Brun, N. E. (2006). *J. Biol. Chem.* **281**, 35467–35477.
Loferer, H., Wunderlich, M., Hennecke, H. & Glockshuber, R. (1995). *J. Biol. Chem.* **270**, 26178–26183.
Martin, J. L. (1995). *Structure*, **3**, 245–250.
Martin, J. L., Bardwell, J. C. & Kuriyan, J. (1993). *Nature (London)*, **365**, 464–468.
Martinou, J. C., Desagher, S. & Antonsson, B. (2000). *Nature Cell Biol.* **2**, E41–E43.
McCarthy, A. A., Haebel, P. W., Törrönen, A., Rybin, V., Baker, E. N. & Metcalf, P. (2000). *Nature Struct. Biol.* **7**, 196–199.
Metheringham, R., Tyson, K. L., Crooke, H., Missiakas, D., Raina, S. & Cole, J. A. (1996). *Mol. Gen. Genet.* **253**, 95–102.
Mieyal, J. J., Starke, D. W., Gravina, S. A. & Hocevar, B. A. (1991). *Biochemistry*, **30**, 8883–8891.
Missiakas, D., Schwager, F. & Raina, S. (1995). *EMBO J.* **14**, 3415–3424.
Mohorko, E., Abicht, H. K., Bühler, D., Glockshuber, R., Hennecke, H. & Fischer, H. M. (2012). *FEBS Lett.* **586**, 4094–4099.
Möller, M. C. & Hederstedt, L. (2008). *J. Bacteriol.* **190**, 4660–4665.
Monika, E. M., Goldman, B. S., Beckman, D. L. & Kranz, R. G. (1997). *J. Mol. Biol.* **271**, 679–692.
Moore, G. R. & Pettigrew, G. W. (1990). *Cytochromes c: Evolutionary, Structural and Physicochemical Aspects.* New York: Springer.
Mössner, E., Huber-Wunderlich, M. & Glockshuber, R. (1998). *Protein Sci.* **7**, 1233–1244.
Murshudov, G. N., Skubák, P., Lebedev, A. A., Pannu, N. S., Steiner, R. A., Nicholls, R. A., Winn, M. D., Long, F. & Vagin, A. A. (2011). *Acta Cryst.* D**67**, 355–367.
Nelson, J. W. & Creighton, T. E. (1994). *Biochemistry*, **33**, 5974–5983.
Nicholson, D. W., Köhler, H. & Neupert, W. (1987). *Eur. J. Biochem.* **164**, 147–157.
Noda, L. H., Kuby, S. A. & Lardy, H. A. (1953). *J. Am. Chem. Soc.* **75**, 913–917.
Otwinowski, Z. & Minor, W. (1997). *Methods Enzymol.* **276**, 307–326.
Ouyang, N., Gao, Y.-G., Hu, H.-Y. & Xia, Z.-X. (2006). *Proteins*, **65**, 1021–1031.
Page, M. D. & Ferguson, S. J. (1997). *Mol. Microbiol.* **24**, 977–990.
Page, M. D., Sambongi, Y. & Ferguson, S. J. (1998). *Trends Biochem. Sci.* **23**, 103–108.
Paxman, J. J., Borg, N. A., Horne, J., Thompson, P. E., Chin, Y., Sharma, P., Simpson, J. S., Wielens, J., Piek, S., Kahler, C. M., Sakellaris, H., Pearce, M., Bottomley, S. P., Rossjohn, J. & Scanlon, M. J. (2009). *J. Biol. Chem.* **284**, 17835–17845.
Pettigrew, G. W. & Moore, G. R. (1987). *Cytochromes c: Biological Aspects*. New York: Springer.
Prakash, S. K., Cormier, T. A., McCall, A. E., Garcia, J. J., Sierra, R., Haupt, B., Zoghbi, H. Y. & Van Den Veyver, I. B. (2002). *Hum. Mol. Genet.* **11**, 3237–3248.
Quan, S., Schneider, I., Pan, J., Von Hacht, A. & Bardwell, J. C. (2007). *J. Biol. Chem.* **282**, 28823–28833.
Reinemer, P., Dirr, H. W., Ladenstein, R., Huber, R., Lo Bello, M., Federici, G. & Parker, M. W. (1992). *J. Mol. Biol.* **227**, 214–226.
Ren, G., Stephan, D., Xu, Z., Zheng, Y., Tang, D., Harrison, R. S., Kurz, M., Jarrott, R., Shouldice, S. R., Hiniker, A., Martin, J. L., Heras, B. & Bardwell, J. C. (2009). *J. Biol. Chem.* **284**, 10150–10159.
Roberts, B. R., Wood, Z. A., Jönsson, T. J., Poole, L. B. & Karplus, P. A. (2005). *Protein Sci.* **14**, 2414–2420.
Roos, G., Foloppe, N. & Messens, J. (2013). *Antioxid. Redox Signal.* **18**, 94–127.
Rost, J. & Rapoport, S. (1964). *Nature (London)*, **201**, 185.
Rozhkova, A., Stirnimann, C. U., Frei, P., Grauschopf, U., Brunisholz, R., Grütter, M. G., Capitani, G. & Glockshuber, R. (2004). *EMBO J.* **23**, 1709–1719.
Sanders, C., Turkarslan, S., Lee, D.-W. & Daldal, F. (2010). *Trends Microbiol.* **18**, 266–274.
Schaefer, L., Ballabio, A. & Zoghbi, H. Y. (1996). *Genomics*, **34**, 166–172.
Schwarz, Q. P. & Cox, T. C. (2002). *Genomics*, **79**, 51–57.
Scott, R. A. & Mauk, A. G. (1995). *Cytochrome c: A Multidisciplinary Approach*. Mill Valley: University Science Books.
Sharma, C. M., Hoffmann, S., Darfeuille, F., Reignier, J., Findeiss, S., Sittka, A., Chabas, S., Reiche, K., Hackermüller, J., Reinhardt, R., Stadler, P. F. & Vogel, J. (2010). *Nature (London)*, **464**, 250–255.
Simon, J. & Hederstedt, L. (2011). *FEBS J.* **278**, 4179–4188.
Stirnimann, C. U., Rozhkova, A., Grauschopf, U., Böckmann, R. A., Glockshuber, R., Capitani, G. & Grütter, M. G. (2006). *J. Mol. Biol.* **358**, 829–845.
Sun, X. X. & Wang, C. C. (2000). *J. Biol. Chem.* **275**, 22743–22749.
Thöny-Meyer, L. (1997). *Microbiol. Mol. Biol. Rev.* **61**, 337–376.
Tian, G., Xiang, S., Noiva, R., Lennarz, W. J. & Schindelin, H. (2006). *Cell*, **124**, 61–73.
Tsukita, S., Koyanagi, S., Nagata, K., Koizuka, H., Akashi, H., Shimoyama, T., Tamura, T. & Sone, N. (1999). *J. Biochem.* **125**, 194–201.
Turkarslan, S., Sanders, C., Ekici, S. & Daldal, F. (2008). *Mol. Microbiol.* **70**, 652–666.
Uchida, K., Mori, H. & Mizushima, S. (1995). *J. Biol. Chem.* **270**, 30862–30868.
Vestweber, D. & Schatz, G. (1988). *J. Cell Biol.* **107**, 2045–2049.
Yoon, J. Y., Kim, J., Lee, S. J., Kim, H. S., Im, H. N., Yoon, H.-J., Kim, K. H., Kim, S.-J., Han, B. W. & Suh, S. W. (2011). *FEBS Lett.* **585**, 3862–3867.
Zhang, M., Monzingo, A. F., Segatori, L., Georgiou, G. & Robertus, J. D. (2004). *Acta Cryst.* D**60**, 1512–1518.
Zollner, A., Rödel, G. & Haid, A. (1992). *Eur. J. Biochem.* **207**, 1093–1100.